Extended Frequency Divider for Bus Frequency Estimation Considering Virtual Inertia from DFIGs

Bendong Tan, Junbo Zhao, Federico Milano, Qiupin Lai, Yingchen Zhang, Daniel Adrian Maldonado

***Abstract*—Accurate estimation of local bus frequency is important for effectively controlling both synchronous and nonsynchronous generators. As the power grid evolves to accommodate essential reliability services such as virtual inertia from nonsynchronous generators, conventional techniques to estimate frequency face challenges. This paper proposes a new frequency estimation method that can effectively include the inertia contributions from double-fed wind generators (DFIGs). This is achieved through the proposed extended frequency divider formula (FDF) to include the contributions of DFIGs via Thevenin equivalents. The proposed extended FDF does not suffer from numerical issues as compared to existing phasor angle derivative-based approaches. Moreover, the knowledge of the rotor speeds of the synchronous machine and DFIGs as well as of the network admittance matrix allows estimating the frequencies of all buses in the grid, thereby significantly improving system situational awareness with a limited number of measurements. Numerical results on the IEEE 39-bus power system with DFIGs show that the proposed method achieves more accurate bus frequency estimations than the original FDF formula and other approaches based on the numerical derivation of the bus voltage phase angles.**

***Keywords*—Frequency estimation, double-fed induction generator (DFIG), Thevenin equivalent, inertial emulation.**

I. Introduction

The penetration of power electronics-interfaced distributed energy resources (DERs), such as DFIGs and solar farms, leads to the inertia reduction in the system. This might lead to the unintended triggering of over/under frequency relays, load shedding, and special protection schemes. Indeed, if the available inertia is low, the rate of change of frequency (ROCOF) can reach unacceptable levels and might lead to cascading failures and blackouts. A relevant example is the Australian blackout in 2016 and the British blackout in 2019 [1]. To mitigate the dynamic issue arising in low-inertia systems, DERs can be equipped with inertia emulation [2].

To enable this emulation requires accurate estimation of frequencies at the buses of DERs. A common way to estimate local bus frequency is to take the numerical derivative of its phase angle measurement. This kind of frequency estimation method is widely used in phasor measurement units (PMUs) after Fourier transformation based phasor estimation [4]. However, numerical derivatives show undesirable spikes due to the sudden changes in bus voltage angles after a disturbance. These spikes may lead to instability when used in the frequency measurement-based control schemes. The phase-locked loop (PLL) [6] is an alternative approach to calculate the local bus frequency, but its performance may deteriorate under harmonics and unbalance.

B. Tan and J. Zhao are with the Department of Electrical and Computer Engineering, Mississippi State University, Starkville, MS 39762. F. Milano is with the School of Electrical and Electronic Engineering, University College Dublin, Dublin, Ireland. Q. Lai is with Electrical Engineering and Automation, Wuhan University, Wuhan, China. Y. Zhang is with the National Renewable Energy Laboratory, Golden, CO 80401, USA. D. Maldonado is with Argonne National Laboratory, Lemont, IL 60439. E-mail: junbo@ece.msstate.edu.

Both frequency estimation methods above rely on phasor measurements to obtain local bus frequency and thus are inevitably influenced by noises and communication losses. To overcome these drawbacks, some analytical methods have been developed. In [7], a model-based derivation for local frequency calculation is proposed but it requires comprehensive and accurate power system dynamic models. These issues have been addressed by the frequency divider formula (FDF), which only needs the knowledge of generator rotor speeds, internal generator impedances, and the standard network admittance matrix [8]. In [8], the spatial variation of frequency in each bus is determined by synchronous machine rotor speeds from simulations. To overcome this limitation, [9] proposes an approach that allows the online implementation of FDF. This is achieved through a hierarchical distributed scheme, where dynamic state estimation is used to estimate the generator rotor speeds using local measurements provided by PMUs or digital fault recorders. Then, these estimates are communicated to a central coordinator for bus frequency estimation with the FDF.

Both references [8] and [9] rely on the assumption that the only devices that can modify the frequency at their point of connection with the grid are synchronous machines. The dynamics and frequency control of DERs are neglected and, hence, frequency estimations might not be fully accurate. Indeed, if DERs are equipped with inertia emulation capabilities, they can provide an inertial response after major contingency and also participate in primary frequency response leading to smaller ROCOF and higher frequency nadir. In other words, the spatial variation of frequency at each bus is affected by the inertia emulation of DERs, which is not accounted for in conventional techniques.

This paper fills this gap and proposes an online bus frequency estimation method considering inertia contributions from DERs. The main contribution of this work is the formulation of an extended frequency divider (FDF) to include the virtual inertia contributions from DERs. In this paper, we focus on double-fed wind generators (DFIGs), to improve frequency estimation accuracy in the presence of large disturbances. In particular, the Thevenin equivalent models of DFIGs are derived and included in the FDF framework. This allows us to model the relationships between generator rotor speeds, including both synchronous machines and DFIGs with virtual inertia, and bus frequencies. The extended FDF only requires a small set of measurements, namely the frequencies at the bus of synchronous machines and DFIGs with inertia emulation, to estimate the frequencies of all buses included in the network. This means that only a reduced number of PMUs are required to estimate bus frequencies. This is economically attractive since the number of generators is typically much smaller than the total number of network buses.

The remainder of the paper is organized as follows. Section II introduces the problem formulation. The proposed extended FDF considering inertia emulation from DFIGs is derived in section III. Section IV presents and analyzes

simulation results on the IEEE 39-bus power system. Conclusions are drawn in section V.

II. Frequency Divider Formula

Typically, the occurrence of a disturbance, such as a load shedding, generator tripping, and three-phase short circuit fault, causes an imbalance between mechanical power and electrical power. This instantaneous imbalance is offset by the synchronous generators' inertia, thereby helping system frequency stability. Specifically, an increase or decrease of rotor speed occurs to re-synchronize synchronous generators with the rest of the power system, which causes rotor angle oscillations. These oscillations disturb the voltage phase angle of the terminal bus at each synchronous generator, leading to unbalanced power. Consequently, the oscillations propagate throughout the entire power system. It can be concluded that the power balance and the consequent frequency deviation at each local bus has a strong relationship with the rotor speed deviation of synchronous generators. To obtain the spatial frequency at each local bus, a boundary value problem can be formulated, where the boundary conditions are determined by rotor speeds of all synchronous generators [8].

According to the discussion above, the spatial frequency at each local bus can be characterized by instantaneous rotor speed estimates of all synchronous generators. This can be described by the original FDF developed in [8]. Specifically, the analytical expression between bus frequencies and rotor speeds of synchronous generators is as follows:

$$diag\left(\boldsymbol{\omega}_B-\omega_0\right)\boldsymbol{V}_B=\mathbf{D}\cdot diag\left(\boldsymbol{\omega}_G-\omega_0\right)\boldsymbol{E}_G \tag{1}$$

where $\boldsymbol{E}_G$ and $\boldsymbol{V}_B$ are respectively generator internal electromotive forces (emfs) and bus voltages; $\mathbf{D}=-\left(\mathbf{Y}_{BB}+\mathbf{Y}_{B0}\right)^{-1}\mathbf{Y}_{BG}$; $\mathbf{Y}_{BB}$ is the network admittance matrix and $\mathbf{Y}_{BG}$ is the bus to generator admittance matrix; $\mathbf{Y}_{B0}$ is a diagonal matrix with the internal impedances of synchronous generators at generator buses; $\boldsymbol{\omega}_B$ and ω_0 are the bus frequency and reference angular frequency while $\boldsymbol{\omega}_G$ are the rotor speeds of synchronous generators.

The FDF shown in (1) provides a simple yet effective way of estimating all system buses with the knowledge of synchronous machine rotor speeds that can be obtained via dynamic state estimation [9]. However, inertia contributions from DERs are neglected and this leads to estimation bias as shown later. Indeed, via virtual inertia control, DFIGs can release kinetic energy stored in the rotor to prevent frequency from decreasing or absorb kinetic energy to stop frequency from increasing. As a result, DFIGs with inertia emulation can provide a frequency response similar to a synchronous generator. More importantly for the objectives of this work, the bus frequency deviation at the buses where DFIGs are connected is a function of the inertia emulation provided by these devices. Thus, the original FDF needs to be extended to include the virtual inertia contributions from DFIGs.

III. Extended FDF with DFIGs

The Thevenin equivalent of DFIG is first presented, followed by the derivations of the analytical relationship between bus frequency and rotor speeds of synchronous generators and DFIGs.

A. Thevenin Equivalent Model of DFIG

To obtain the extended FDF considering inertial contributions from DFIGs, the Thevenin equivalent of each DFIG is required. This section shows the derivations of such an equivalent. The induction generator, rotor side converter (RSC) and grid side converter (GSC) are also briefly discussed.

According to [10], if the effects of RSC and GSC are considered, the Thevenin equivalent impedance of the DFIG Z_{DFIG} seen from its terminal can be denoted as:

$$Z_{DFIG}(s)=Z_1\,//\,(Z_{GSC}+L_f s) \tag{2}$$

$$Z_1=[r_r/\text{slip}(s)+L_{lr}s+Z_{RSC}/\text{slip}(s)]\,//\,L_m s+r_s+L_{ls}s \tag{3}$$

where r_r is the rotor resistance; r_s is the stator resistance; Z_{RSC} is the impedance of RSC, and s is the Laplacian operator; L_{lr} and L_{ls} are respectively the leakage inductance of rotor and stator; L_f represents the inductive filter at GSC; L_m is the magnetizing inductance; slip(s) is the slip of induction generator in Laplace domain:

$$\text{slip}(s)=\frac{s-j\omega_R}{s} \tag{4}$$

and ω_R is the rotor speed of DFIG.

Therefore, the impedances of RSC and GSC are

$$Z_{RSC}=H(s-j\omega_0)-jK_d \tag{5}$$

$$Z_{GSC}=H(s-j\omega_0)-jK_d \tag{6}$$

where $H(s)=K_p+\frac{K_i}{s}$; K_p is the proportional gain; K_i and K_d are the integral gain and compensation gain, respectively. The voltage sources behind them are respectively $I_r^*H(s-j\omega_0)$ and $I_g^*H(s-j\omega_0)$, where I_r^* is the reference current in RSC and I_g^* is the reference current in GSC. With a constant dc bus voltage between RSC and GSC, the dynamics of the GSC and RSC are uncoupled [11]. Therefore, the overall circuit is now shown in Fig. 1.

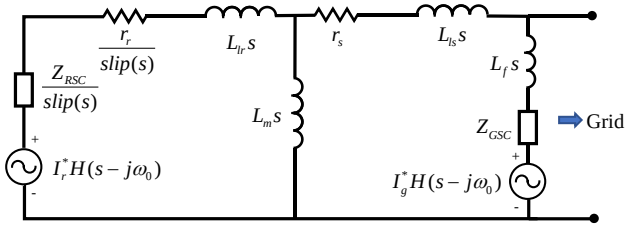

Fig. 1. The electric circuit of DFIG considering virtual inertia control.

Thus, according to Fig. 1, the Thevenin equivalent potential E_R can be calculated as follows:

$$E_R=I_r^*H(s-j\omega_0)\left[\frac{Z_a\,//\,L_m s}{Z_a\,//\,L_m s+Z_b}\frac{L_f s+Z_{GSC}}{Z_a}\right]+I_g^*H(s-j\omega_0)\frac{Z_b\,//\,L_m s+r_s+L_{ls}s}{Z_b\,//\,L_m s+Z_a} \tag{7}$$

$$Z_a=r_s+L_{ls}s+L_m s+Z_{GSC} \tag{8}$$

$$Z_b=r_r/slip(s)+L_{lr}s+Z_{RSC}/slip(s) \tag{9}$$

The inertia emulation of DFIG considered in this paper is the droop control based on frequency deviation, which can be expressed as [12]:

$$\Delta P = -R\Delta f \tag{10}$$

where ΔP is the deviation of reference active power of DFIG; R is the droop gain and Δf is the frequency deviation at the bus where DFIG is connected to. Since I_r^* varies due to ΔP, ΔP only changes E_R. Therefore, (2) and (7) are sufficient to calculate the Thevenin equivalent model of DFIG no matter the inertia emulation is equipped or not.

B. Frequency Divider Formula with DFIGs

Electromechanical oscillations can be depicted by the magnitude and phase angle modulations of voltages and currents because they are closely related to the rotor speed deviation of synchronous generators [13]. Thus, to include the inertia contributions from DFIGs into the FDF framework, the relationship of the voltage or current phasors between generators and system buses should be firstly built, which can be expressed as:

$$\begin{bmatrix} \boldsymbol{I}_G \\ \boldsymbol{I}_R \\ \boldsymbol{I}_B \end{bmatrix} = \begin{bmatrix} \mathbf{Y}_{GG} & & \mathbf{Y}_{GB} \\ & \mathbf{Y}_{RR} & \mathbf{Y}_{RB} \\ \mathbf{Y}_{BG} & \mathbf{Y}_{BR} & \mathbf{Y}_{BB}+\tilde{\mathbf{Y}}_{B0} \end{bmatrix} \begin{bmatrix} \boldsymbol{E}_G \\ \boldsymbol{E}_R \\ \boldsymbol{V}_B \end{bmatrix} \tag{11}$$

where $\boldsymbol{I}_G$, $\boldsymbol{I}_R$ and $\boldsymbol{I}_B$ are respectively current injections from synchronous generators, DFIGs and loads; $\mathbf{Y}_{GG}$ is the admittance matrix obtained by utilizing the internal impedances of synchronous generators at generator buses; $\mathbf{Y}_{RR}$, $\mathbf{Y}_{BR}$ and $\mathbf{Y}_{RB}$ are admittance matrices obtained by utilizing the Thevenin equivalent impedances of DFIGs; $\tilde{\mathbf{Y}}_{B0}$ is a diagonal matrix, which is calculated with the internal impedances of synchronous generators and the Thevenin equivalent impedances of DFIGs.

Since the equivalent load admittance is smaller than the diagonal elements of $\mathbf{Y}_{BB}+\tilde{\mathbf{Y}}_{B0}$, load current injections are neglected. This assumption has been used in [8] and extensive numerical results carried out demonstrate that it does not affect the accuracy of the FDF. Thus, (11) is rewritten as:

$$\begin{bmatrix} \boldsymbol{I}_G \\ \boldsymbol{I}_R \\ \mathbf{0} \end{bmatrix} = \begin{bmatrix} \mathbf{Y}_{GG} & & \mathbf{Y}_{GB} \\ & \mathbf{Y}_{RR} & \mathbf{Y}_{RB} \\ \mathbf{Y}_{BG} & \mathbf{Y}_{BR} & \mathbf{Y}_{BB}+\tilde{\mathbf{Y}}_{B0} \end{bmatrix} \begin{bmatrix} \boldsymbol{E}_G \\ \boldsymbol{E}_R \\ \boldsymbol{V}_B \end{bmatrix} \tag{12}$$

Then, the analytical relationships between $\boldsymbol{E}_R$, $\boldsymbol{E}_G$ and bus voltages can be derived as:

$$\boldsymbol{V}_B = -\left(\mathbf{Y}_{BB}+\tilde{\mathbf{Y}}_{B0}\right)^{-1}\begin{bmatrix}\mathbf{Y}_{BG} & \mathbf{Y}_{BR}\end{bmatrix}\begin{bmatrix}\boldsymbol{E}_G \\ \boldsymbol{E}_R\end{bmatrix} = \tilde{\mathbf{D}}\begin{bmatrix}\boldsymbol{E}_G \\ \boldsymbol{E}_R\end{bmatrix} \tag{13}$$

Applying time derivatives on both sides of (13), the following formula can be obtained:

$$\frac{d\boldsymbol{V}_B}{dt} + j\omega_0\boldsymbol{V}_B = \tilde{\mathbf{D}}\begin{bmatrix}\dfrac{d\boldsymbol{E}_G}{dt} \\ \dfrac{d\boldsymbol{E}_R}{dt}\end{bmatrix} + j\omega_0\tilde{\mathbf{D}}\begin{bmatrix}\boldsymbol{E}_G \\ \boldsymbol{E}_R\end{bmatrix} \tag{14}$$

According to [8], the following assumptions can be made:

$$\begin{cases} \dfrac{dV_{B,i}}{dt} \approx j\omega_{B,i}V_{B,i} \\ \dfrac{dE_{G,k}}{dt} \approx j\omega_{G,k}E_{G,k} \\ \dfrac{dE_{R,l}}{dt} \approx j(\omega_{R,l}-\omega_{F,l})E_{R,l} \end{cases} \text{ and } \begin{cases} \omega_{B,i}=\omega_0+\Delta\omega_{B,i} \\ \omega_{G,k}=\omega_0+\Delta\omega_{G,k} \\ \omega_{R,l}=\omega_{R0,l}+\Delta\omega_{R,l} \end{cases} \tag{15}$$

where $\omega_{B,i}$ and $V_{B,i}$ are respectively the angular frequency and voltage amplitude of bus i; $\omega_{G,k}$ and $E_{G,k}$ are respectively the rotor speed and emf of synchronous generator k; $\omega_{R,l}$, $\omega_{F,l}$ and $E_{R,l}$ are respectively the rotor speed, the rotor excitation angular frequency and Thevenin equivalent potential of DFIG l; $\omega_{R0,l}$ is the value of $\omega_{R,l}$ in the steady-state. Merging (13), (14), and (15) leads to:

$$diag\left(\boldsymbol{\omega}_B-\boldsymbol{\omega}_0\right)\boldsymbol{V}_B = \tilde{\mathbf{D}}\cdot diag\left(\begin{bmatrix}\boldsymbol{\omega}_G-\boldsymbol{\omega}_0 \\ \boldsymbol{\omega}_R-\boldsymbol{\omega}_{R0}\end{bmatrix}\right)\begin{bmatrix}\boldsymbol{E}_G \\ \boldsymbol{E}_R\end{bmatrix} \tag{16}$$

It is noticeable that the conductance of the elements of all admittance matrices used to compute $\tilde{\mathbf{D}}$ is small enough to be neglected. The following assumptions are made in [8]:

$$\boldsymbol{V}_B \approx \mathbf{1}\text{ p.u. and }\boldsymbol{E}_G \approx \mathbf{1}\text{ p.u.} \tag{17}$$

However, if $\boldsymbol{V}_B$ and $\boldsymbol{E}_G$ are available from estimations, or PMUs, or other devices, we can use their online values.

IV. Numerical Results

This section demonstrates the effectiveness of the proposed FDF considering DFIGs using simulations on the IEEE 39-bus system. The network is shown in Fig. 2 and details of adding DFIGs will be shown later. All simulations are carried out using DIgSILENT PowerFactory.

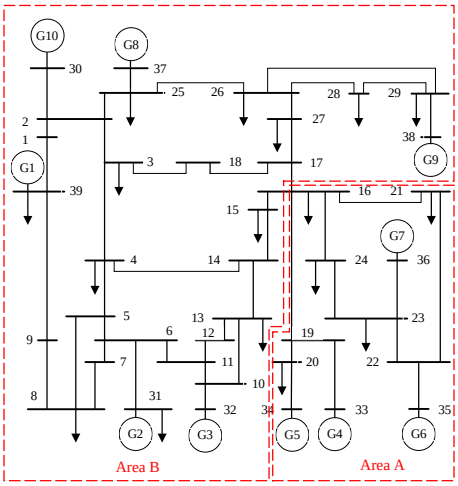

Fig. 2. The single-line diagram of the IEEE 39-bus power system.

Three scenarios are considered in this paper. The disturbances are all three-phase faults that occur at 1 s and are cleared at 1.1s. The parameters of each wind turbine are shown in Table I. The per-unit value of each wind turbine parameter is based on the rated power of 5 MW with a rated voltage of 0.69 kV. Since the stator frequency of each DFIG turbine is unknown, the angular frequency of the center of inertia ω_{COI} for the entire wind farm is utilized to calculate s, yielding $s = j(\omega_{COI}-\omega_0)$ [11]. The synchronous reference frame PLL (SRF–PLL) is the simplest and the most

commonly used scheme for frequency estimation of DERs [14]. Therefore, the SRF-PLL is utilized for comparison with other frequency estimation methods. DIgSILENT PowerFactory also provides a frequency estimation which is a washout filter. The frequency estimation results from DIgSILENT PowerFactory as well as the original FDF are also utilized for comparisons.

TABLE I. PARAMETERS OF EACH WIND TURBINE

Parameters	*Value (p.u.)*	*Parameters*	*Value*
r_s	0.01	K_p	0.0496
L_{lr}	0.1	K_i	0.0128
L_{ls}	0.1	K_d	0
L_f	0		
L_m	3.5		

A. FDF without Inertia Emulation of DFIGs

Scenario 1: The G10 is replaced by DFIG1 of 250 MW with 50 wind turbines. The inertia emulation is not considered in this scenario to assess the frequency estimation accuracy of each method. The three-phase fault is applied to bus 16. This bus connects the areas A and B of the IEEE 39-bus system, thus a three-phase fault at this bus leads to large disturbance and, in turn, to large frequency deviations.

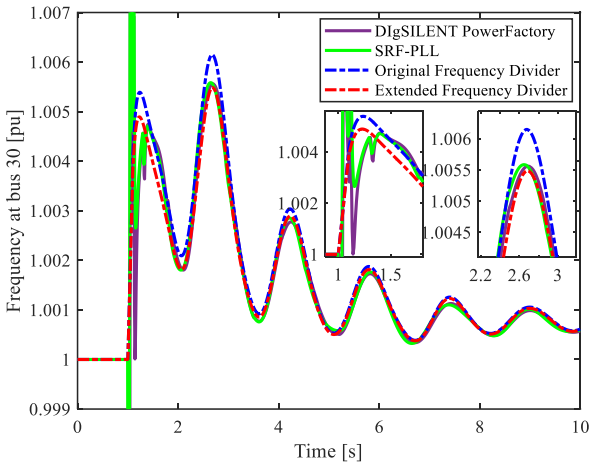

Fig. 3. Estimated frequency at bus 30 by different methods in scenario 1.

The estimated frequency at bus 30 by each method is shown in Fig. 3. The results obtained with DIgSILENT PowerFactory and SRF–PLL suffer from spikes when the disturbance occurs. This is typical of all methods that involve some sort of numerical derivative of bus voltage phase angles. On the other hand, both the original FDF and the proposed formulation avoid spikes. The rotor speeds of synchronous machines and DFIGs are state variables and, as such, cannot change instantaneously. The FDF builds the analytical relationships between bus frequencies and those rotor speeds. Therefore, the bus frequencies calculated from rotor speeds are not subject to sudden changes. After the initial spike, it is interesting to observe that the extended FDF has closer results as those from DIgSILENT PowerFactory and SRF–PLL than the original FDF after disturbances. This is because DFIG still provides some inertial response though DFIG is not equipped with inertia emulation due to the PLL synchronization scheme [15]. As a result, the extended FDF implicitly captures the small inertial response and contributes to the variation in the estimation of spatially distributed bus frequencies.

Figs. 4(a) and 4(b) show the Thevenin equivalent potential value and impedance of DFIG1, respectively, during the transient process in Scenario 1. These two values change due to the inertial response although being very small. Therefore, they cannot be treated as constants. Neglecting these variations affects the frequency estimation, as shown by the comparisons between the original and extended FDFs.

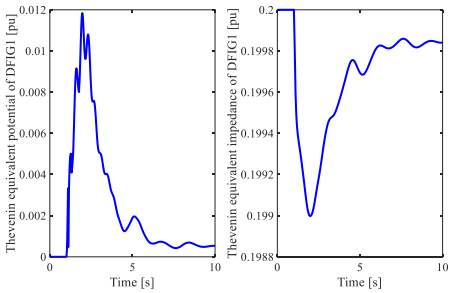

(a) (b)

Fig. 4. Thevenin equivalent of DFIG1 during the transient process in scenario 1. (a) Equivalent potential value. (b) Equivalent impedance.

B. FDF with Inertia Emulation of DFIGs

Scenario 2: The settings are similar to Scenario 1, where G10 is replaced by DFIG1 but the droop control-based inertia emulation is considered with a droop coefficient R of 2.

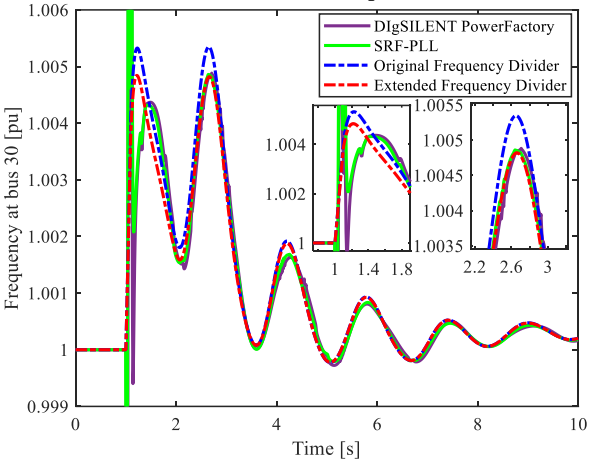

Fig. 5. Estimated frequency at bus 30 by different methods in scenario 2.

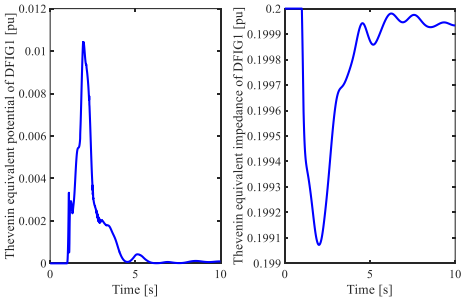

(a) (b)

Fig. 6. Thevenin equivalent of DFIG1 during the transient process in scenario 2. (a) Equivalent potential value. (b) Equivalent impedance.

The frequency estimations at bus 30 by the four methods are presented in Fig. 5. The magnitude of bus frequency has been reduced for both the original and extended FDFs. For the original FDF, due to the activation of inertial emulation, the system has more frequency support and the synchronous machines have reduced rotor speed deviations. This results in

the reduced magnitude of the bus frequency. Although the original FDF can capture the impact of inertial emulation control, it is still subject to estimation biases as compared to the extended FDF. Again, since it neglects the contributions of DFIGs to frequency deviations, the original FDF does not achieve similar accuracy as those by DIgSILENT PowerFactory and SRF–PLL.

Figs. 6 (a) and 6(b) show the Thevenin equivalent potential value and impedance of DFIG1, respectively, during the transient process in Scenario 2. With inertial control, DFIG1 reduces more active power than the one without it, leading to larger rotor speed deviation. As a result, DFIG1 has smaller Thevenin equivalent potential but larger equivalent impedance as compared to Scenario 1.

C. *Multiple Wind Farms Considering Inertia Emulation*

Scenario 3: G10 and G5 are respectively replaced with DFIG1 and DFIG2, and the power capacity of DFIG2 with 100 wind turbines is 500 MW. Inertia emulation is implemented for both DFIGs. The droop coefficient R is set to 1 in both DFIGs.

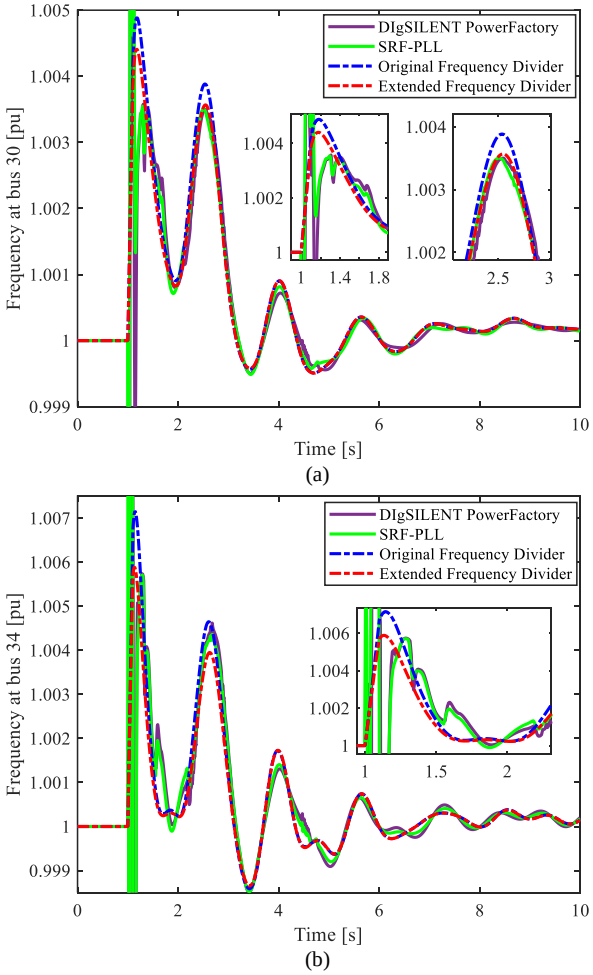

Fig. 7. Frequency estimation results in scenario 3. (a) Estimated frequency at bus 30. (b) Estimated frequency at bus 34.

The estimated frequencies at buses 30 and 34 are plotted in Figs. 7(a) and 7(b), respectively. Simulation results are consistent with those obtained for Scenarios 1 and 2. An interesting observation is that, with the increased penetration of DFIGs, the fluctuations in the system becomes more violent, causing more severe spikes in the frequency estimation results from DIgSILENT PowerFactory and SRF–PLL. If the controls are designed based on these inaccurate frequency estimates, the controller may show instability issues. The extended FDF is thus more suitable for local frequency estimation than other methods especially in systems with high penetration of DFIGs.

V. Conclusion

An extended FDF is proposed to include the inertia emulation contributions from DFIGs. With this aim, a Thevenin equivalent model of DFIGs is derived and is duly included in the formulation of the FDF. This allows building an analytical relation between the rotor speeds of DFIGs and synchronous generators and bus frequencies. Simulation results carried out on the IEEE 39-bus system show that the proposed method yields a more accurate and robust frequency estimation than existing methods. In future work, we will test the proposed method under different inertia emulation schemes and larger-scale systems with different penetration levels of DERs and energy storage systems.

References

[1] F. Milano, F. Dörfler, G. Hug, D. J. Hill and G. Verbič, "Foundations and Challenges of Low-Inertia Systems (Invited Paper)," *2018 Power Systems Computation Conference*, Dublin, Ireland, pp. 1-25, 2018.

[2] W. Bao, Q. Wu, L. Ding, S. Huang and V. Terzija, "A hierarchical inertial control scheme for multiple wind farms with BESSs based on ADMM," *IEEE Trans. Sustainable Energy*, 2020, in press.

[3] A. Hosseinipour and H. Hojabri, "Virtual inertia control of PV systems for dynamic performance and damping enhancement of DC microgrids with constant power loads," *IET Renewable Power Generation*, vol. 12, no. 4, pp. 430-438, Mar. 2018.

[4] IEEE TF on Load Representation for Dynamic Performance, "Load representation for dynamic performance analysis of power systems," *IEEE Trans. Power System*, vol. 8, no. 2, pp. 472–482, May. 1993.

[5] I. Kamwa, M. Leclerc and D. McNabb, "Performance of demodulation-based frequency measurement algorithms used in typical PMUs," *IEEE Trans. Power Delivery*, vol. 19, no. 2, pp. 505-514, Apr. 2004.

[6] M. Lai, M. Nakano, and G. Hsieh, "Application of fuzzy logic in the phase-locked loop speed control of induction motor drive," *IEEE Trans. Industrial Electronics*, vol. 43, no. 6, pp. 630–639, Dec., 1996.

[7] J. Nutaro and V. Protopopescu, "Calculating frequency at loads in simulations of electro-mechanical transients," *IEEE Trans. Smart Grid*, vol. 3, no. 1, pp. 233–240, Mar. 2012.

[8] F. Milano and A. Ortega, "Frequency divider," *IEEE Trans. Power Systtem*, vol. 32, no. 2, pp. 1493–1501, Mar. 2017.

[9] J. Zhao, L. Mili and F. Milano, "Robust frequency divider for power system online monitoring and control," *IEEE Trans. Power Systems*, vol. 33, no. 4, pp. 4414-4423, Jul. 2018.

[10] Z. Miao, "Impedance-model-based SSR analysis for Type 3 wind generator and series-compensated network," *IEEE Trans. Energy Conversion*, vol. 27, no. 4, pp. 984-991, Dec. 2012.

[11] I. Vieto and J. Sun, "Sequence impedance modeling and analysis of Type-III wind turbines," *IEEE Trans. Energy Conversion*, vol. 33, no. 2, pp. 537-545, Jun. 2018.

[12] M. Hwang, E. Muljadi, J. Park, P. Sørensen and Y. C. Kang, "Dynamic droop–based inertial control of a doubly-Ffed induction generator," *IEEE Trans. Sustainable Energy*, vol. 7, no. 3, pp. 924-933, Jul. 2016.

[13] A. G. Phadke and B. Kasztenny, "Synchronized phasor and frequency measurement under transient conditions," IEEE Trans. Power Delivery, vol. 24, no. 1, pp. 89–95, Jan. 2009.

[14] A. Ortega, F. Milano, "Comparison of different PLL implementations for frequency estimation and control," *18th Int. Conf. on Harmonics and Quality of Power*, Ljubljana, Slovenia, pp. 1-6, May. 2018.

[15] J. Van de Vyver, J. D. M. De Kooning, B. Meersman, L. Vandevelde and T. L. Vandoorn, "Droop control as an alternative inertial response strategy for the synthetic inertia on wind turbines," *IEEE Trans. Power Systems*, vol. 31, no. 2, pp. 1129-1138, Mar. 2016.